of the relevant commensurate networks, the main difference being a slight improvement in the "flatness" of gain. In both cases the equalizers designed by optimization have as their first element a UE of characteristic impedance equal to the specified upper limit. This is consistent with predictions made from gain–bandwidth theory applied to the commensurate case.

V. Conclusions

Within the limitations set by the use of approximate models of transistor behavior, a study has been made of the gain–bandwidth restrictions of a distributed-element equalizer with unspecified commensurate length. It has been shown that the greatest gain may be possible with a lumped-element equalizer, while simple commensurate networks can usually be expected to provide near optimum gain. The size problem associated with commensurate networks can be alleviated to some extent by the use of more specialized forms of network, but the problem is considerable in the case of FET's and other devices with high input and output impedance levels. With such devices constraints on characteristic impedance necessitate large equalizer line lengths which, in turn, have a detrimental effect on gain–bandwidth performance.

Acknowledgment

The author wishes to thank D. F. Hewitt for valuable discussions and guidance throughout the course of this work.

References

[1] T. W. Houston and L. W. Read, "Computer-aided design of broad-band and low-noise microwave amplifiers," *IEEE Trans. Microwave Theory Tech. (Special Issue on Computer-Oriented Microwave Practices)*, vol. MTT-17, pp. 612–614, Aug. 1969.
[2] T. N. Trick and J. Vlach, "Computer-aided design of broad-band amplifiers with complex loads," *IEEE Trans. Microwave Theory Tech.*, vol. MTT-18, pp. 541–547, Sept. 1970.
[3] R. M. Fano, "Theoretical limitations on the broad-band matching of arbitrary impedances," *J. Franklin Inst.*, vol. 249, pp. 57–83, Jan. 1950; also pp. 139–154, Feb. 1950.
[4] D. C. Youla, "A new theory of broad-band matching," *IEEE Trans. Circuit Theory*, vol. CT-11, pp. 30–50, Mar. 1964.
[5] R. S. Tucker, "Synthesis of broad-band microwave transistor amplifiers," *Electron. Lett.*, vol. 7, pp. 455–456, Aug. 12, 1971.
[6] R. Levy, "Synthesis of mixed lumped and distributed impedance-transforming filters," *IEEE Trans. Microwave Theory Tech.*, vol. MTT-20, pp. 223–233, Mar. 1972.
[7] H. F. Cooke, "Microwave transistors: Theory and design," *Proc. IEEE (Special Issue on Microwave Semiconductors)*, vol. 59, pp. 1163–1181, Aug. 1971.
[8] H. J. Carlin and R. A. Friedenson, "Gain bandwidth properties of a distributed parameter load," *IEEE Trans. Circuit Theory (Special Issue on Modern Filter Design)*, vol. CT-15, pp. 455–464, Dec. 1968.
[9] K. Hartmann, W. Kotyczka, and M. J. O. Strutt, "Computer-aided determination of the small-signal equivalent network of a bipolar microwave transistor," *IEEE Trans. Microwave Theory Tech.*, vol. MTT-20, pp. 120–126, Feb. 1972.
[10] W. I. Zangwill, "Minimization of a function without calculating derivatives," *Comput. J.*, vol. 10, pp. 293–296, Nov. 1967.
[11] J. W. Bandler, "Optimization methods for computer-aided design," *IEEE Trans. Microwave Theory Tech. (Special issue on Computer-Oriented Microwave Practices)*, vol. MTT-17, pp. 533–552, Aug. 1969.
[12] M. Caulton, B. Hershenov, S. P. Knight, and R. E. DeBrecht, "Status of lumped elements in microwave integrated circuits—Present and future," *IEEE Trans. Microwave Theory Tech. (Special Issue on Microwave Integrated Circuits)*, vol. MTT-19, pp. 588–599, July 1971.

Accurate Determination of Varactor Resistance at UHF and its Relation to Parametric Amplifier Noise Temperature

KUBİLÂY İNAL AND CANAN TOKER

Abstract—**A thorough investigation is made on the frequency-dependent properties of a varactor diode loss resistance at UHF. The variation of the losses with frequency in a varactor diode mounted cavity has been theoretically investigated, and it is shown that the previously reported inverse-squared frequency dependence of the varactor loss resistance can be attributed to the distributed cavity losses transformed across the varactor diode.**

A new measurement technique is introduced in which the circuit losses are first matched to the input line instead of the varactor loss resistance as an application of the relative impedance method. Measurements carried out with this technique for five different varactor diodes showed that the loss resistances of these diodes are not frequency dependent.

It is also shown that the choice of the varactor diode capacitance plays an important role on the parametric amplifier noise temperature at UHF. In an experimental parametric amplifier the effect of varactor diode capacitance on the noise temperature has been demonstrated. It has been theoretically and experimentally shown that, generally, varactor diodes having higher capacitances result in better noise temperature at UHF.

Manuscript received August 4, 1972; revised November 13, 1972. This work was supported in part by the Scientific and Technical Development Council of Turkey (TBTAK).

The authors are with the Department of Electrical Engineering, Middle East Technical University, Ankara, Turkey.

I. Introduction

THE ACCURATE measurement of the varactor diode parameters has been the subject of many research workers for some time. The varactor diode parameters have been measured experimentally starting from lower side of UHF (that is, from 300 MHZ upwards) extending to X band and above. Different methods have been employed, each of which has distinct advantages over the others depending upon the frequency of measurement, components

used as circuit elements, and the type of the varactor diode. Many factors concerning the parameters of the varactor diode have been established, and the different measurement techniques yielded more or less the same results for frequencies higher than about 1 GHz. However, measurements of varactor loss resistance below 1 GHz produced conflicting results, and it has generally been accepted that this resistance varies inversely with the square of frequency [1], [2]. Eng and Solomon [3] and Sawyer [4] pointed out that the frequency dependency was due to the surface effects. The effect of inverse-squared frequency dependence of the apparent resistance of varactor diodes is also discussed in the optimization of the noise figure of negative resistance and up-converter parametric amplifiers [5]. With the currently available varactors it is thought that the surface effects are no longer present and the apparent variation of resistance with frequency may be due to the inaccuracy of the measurement techniques employed [6].

The measurement techniques themselves have received much interest in the past years. Regarding the relative impedance measurement techniques [7], [8], the diode resistance is matched to the input line and suffer largely from the circuit losses. This method can be applied to the upper UHF (that is, 3 GHz and higher) and low microwave frequencies where the circuit losses become less important as will be apparent in the following sections. In any case the circuit losses involved can be taken into account by a method described by Sard [9] and by a numerical data processing technique [10]. The transmission loss measurements developed by DeLoach [11] are not applicable to UHF since all the diodes used for microwave parametric amplifiers have their resonant frequencies above 5 GHz. The series resonance method [12] again gives inconsistent results due to the rather complicated transformations of the diode mount [13] and the short-circuit resistance, caused by the equivalent circuit parameters.

In the next section the distributed cavity losses of a varactor mounted cavity are evaluated. A new measurement technique is described in Section III, and the effect of the cavity losses and the varactor diode stray elements on the circulator coupled parametric amplifier noise temperature is discussed in Section IV.

II. Calculation of Circuit Losses

For nearly all measurement purposes and the purpose of parametric amplification, the diode capacitance is tuned out with a short-circuited transmission line. In Fig. 1 the equivalent circuit of a cavity-mounted varactor diode at UHF is shown. In this figure C_j and R_j are the junction capacitance and the loss resistance of the varactor diode, respectively. C_A is the stray capacitance due to the discontinuity of the inner conductor [14] and L_c and R_c are the equivalent inductance and the loss resistance of the cavity, respectively. R_c is the real component of the input impedance of a short-circuited transmission line used to resonate a capacitance value of $C_T = C_A + C_1 + C_2 + C_j$ at a frequency $f = (\omega/2\pi)$, where C_1 and C_2 are the diode package and junction stray capacitances, respectively. In the following analysis the contact resistances are ignored and the losses occurring on the cavity walls and those occurring on the surface of the short-circuiting plate have been investigated. These analyses differ from that of a capacity-loaded reentrant cavity [15] in the sense that C_T is not produced by the cavity dimensions and can have any arbitrary value.

For small losses, to a very good approximation the length

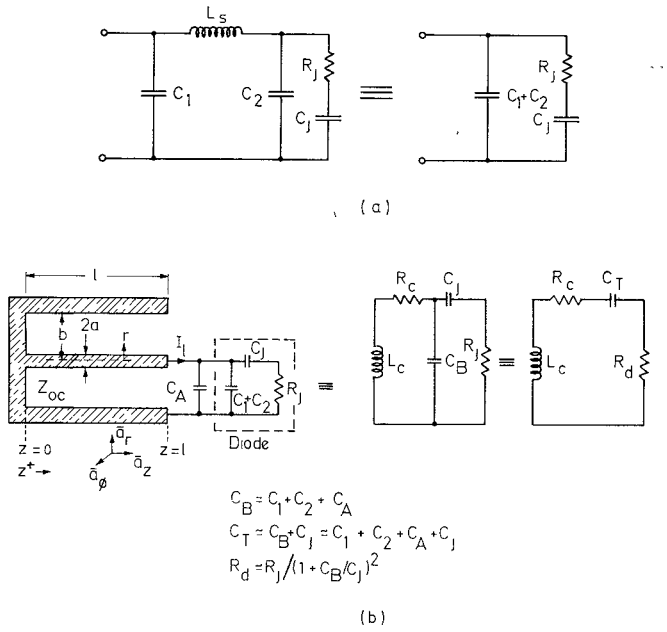

Fig. 1. (a) Representation of varactor diode and its equivalent circuit at UHF. (b) Equivalent circuit of the cavity-mounted varactor diode.

of the cavity l is fixed by

$$\frac{1}{\omega C_T} = Z_{oc} \tan \beta l. \tag{1}$$

Assuming that the total cavity losses are dissipated in a resistance $R_c(\omega)$ connected at $z = l$

$$R_c(\omega) = \frac{P_T}{\frac{1}{2} I_l^2} = \frac{\frac{1}{2} R_m \oint\oint_{\text{walls}} |H_T(r, z)|\, ds}{\frac{1}{2}\left[\oint_c H_T(a, l)\, dc\right]^2} \tag{2}$$

where P_T is the total dissipated power, R_m surface resistance, and I_l total current flowing in the inner conductor at the point $z = l$. For TEM mode the total magnetic field is given by

$$\overline{H}_T(r, z) = \bar{a}_\phi 2Y \frac{K}{r} \cos \beta z \tag{3}$$

where $Y = (\epsilon_0/\mu_0)^{1/2}$ and K is a constant. Now

$$P_T = P_a + P_b + P_0 \tag{4}$$

where subscripts a, b, and 0 indicate the power losses on the inner, outer conductors, and the end plate, respectively. Substituting (3) into (2) the following quantities are obtained:

$$\left.\begin{aligned} P_a &\simeq \frac{2\pi}{a} Y^2 K^2 R_m l \\ P_b &\simeq \frac{2\pi}{b} Y^2 K^2 R_m l \end{aligned}\right\}, \qquad \frac{\sin 2\beta l}{2\beta} \ll l \text{ is assumed} \tag{5, 6}$$

$$P_0 = 4\pi R_m Y^2 K^2 \ln \frac{b}{a} \tag{7}$$

$$I_l^2 = \left[\int_0^{2\pi} H_T(a, l) a\, d\phi\right]^2 = 16\pi^2 Y^2 K^2 \cos^2 \beta l$$

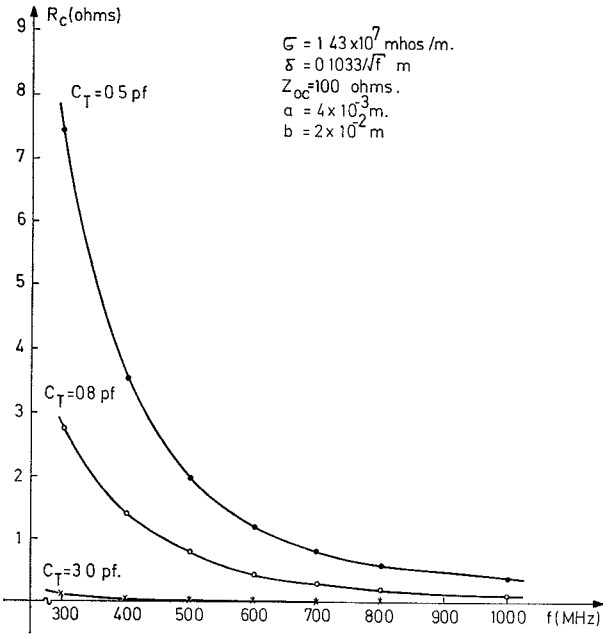

Fig. 2. Variation of cavity loss resistance with frequency for different values of C_T.

$$\simeq \frac{16\pi^2 Y^2 K^2}{\tan^2 \beta l}, \qquad \tan^2 \beta l \gg 1 \text{ is assumed} \quad (8)$$

substituting (5)–(8) and

$$l = \frac{v}{\omega} \tan^{-1}(1/\omega Z_{oc} C_T), \quad R_m = \omega^{1/2} \sqrt{\frac{\mu_0}{2\sigma}} = \frac{1}{\sigma \delta}$$

(σ is the conductivity, δ skin depth, and v velocity of propagation) and

$$\tan^2 \beta l = \frac{1}{\omega^2 C_T^2 Z_{oc}^2}$$

into (2), $R_c(\omega)$ is obtained as

$$R_c(\omega) = \frac{\sqrt{\frac{\mu_0}{2\sigma}}(b+a)v}{4\pi C_T^2 Z_{oc}^2 ab} \left(\frac{1}{\omega^{5/2}}\right) \tan^{-1}\left(\frac{1}{\omega C_T Z_{oc}}\right) + \frac{\ln \frac{b}{a}}{2\pi\sigma\delta\omega^2 C_T^2 Z_{oc}^2}. \quad (9)$$

The second term of the above expression is the loss resistance of the short-circuiting plate transformed to the input of the transmission line and for practical values is negligible as compared to the first term. Variation of $\tan^{-1}(1/\omega C_T Z_{oc})$ in the frequency range 0.5–1 GHz is rather slow as compared to the variation of $(1/\omega^{5/2})$. Hence, the cavity loss resistance can be considered to vary, to a first approximation, inversely with $\omega^{5/2}$. This result may explain the inverse-squared frequency dependence of the apparent resistance of varactor diodes as measured at UHF. In Fig. 2 the variation of cavity loss resistance is plotted for different values of C_T. As is seen, due to the reduced L_e required to resonate C_T at a given ω, the effective loss resistance decreases as C_T increases. In a practical cavity the effective loss resistance is always higher than the idealized case considered here due to the imperfections in the surfaces

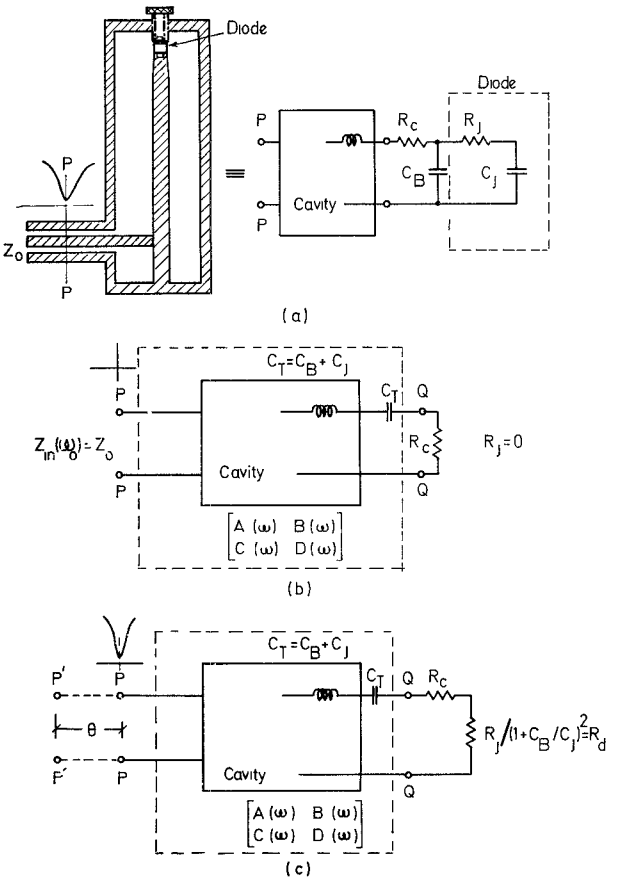

Fig. 3. (a) Setup used for varactor diode loss resistance measurements. (b) Equivalent circuit when the diode is replaced by a lossless capacitance of equal value. (c) Equivalent circuit when the diode is in the cavity.

of the cavity and the contact resistances of the moving parts in a tunable parametric amplifier.

It now remains to show that in an actual measurement, the varactor diode resistance does not depend on frequency. A direct measurement of this resistance, when the diode is mounted in a cavity, always yields results which include the frequency-dependent nature of resistance of the cavity $R_c(\omega)$. In the following section a new method is introduced in which the cavity losses are made ineffective.

III. New Measurement Technique

In all the methods so far developed, using the relative impedance measurement technique, the varactor diode loss resistance, as mounted in a cavity, is matched to the characteristic impedance of the input transmission line. In this matching process the cavity losses are also matched to the input line although the method entirely depends on the assumption that the matching network, i.e., the cavity in this case, is lossless. In the following method first the cavity losses are matched to the input line when the diode is replaced by a lossless capacitance of value equal to the capacitance of the varactor diode. Then using the Weissfloch transformer theorem the transformation ratio due to the lossless part of the cavity is obtained.

The setup used for this measurement technique is shown in Fig. 3. The equivalent circuit of the cavity is represented by an inductance in series with a loss resistance $R_c(\omega)$. The system between the reference plane PP and QQ, as shown in Fig. 3(b), is represented by a 2-port network whose chain

parameters are defined as $A(\omega)$, $B(\omega)$, $C(\omega)$, and $D(\omega)$. In this equivalent circuit C_T is included inside the network but the series loss resistance of the cavity is considered outside. If the coupling to the cavity is so adjusted that when R_c terminates the network a match condition is obtained at the terminals PP at $\omega=\omega_0$ where ω_0 is the resonant frequency, the input impedance at PP then becomes

$$Z_{\text{in}}(\omega_0) = \frac{A(\omega_0)R_c(\omega_0) + B(\omega_0)}{C(\omega_0)R_c(\omega_0) + D(\omega_0)} = Z_o. \tag{10}$$

If $R_c(\omega_0)$ could be made equal to zero, a short-circuit plane at the input line would result. Assuming that the reference plane PP is selected at the point of this short circuit, the equivalent circuit between the planes PP and QQ becomes that of an ideal transformer [16], whose chain matrix is given by

$$\begin{bmatrix} \sqrt{Z_o/R_c(\omega_0)} & 0 \\ 0 & \sqrt{R_c(\omega_0)/Z_o} \end{bmatrix} \tag{11}$$

where $A(\omega_0)=1/D(\omega_0)=\sqrt{Z_o/R_c(\omega_0)}$ is the turn ratio and $B(\omega_0)=C(\omega_0)=0$. Employing (10) and (11) the input impedance at the plane PP is given by [Fig. 3(c)]

$$Z_{\text{in}}(\omega_0) = \frac{Z_o}{R_c(\omega_0)} R_L(\omega_0) \tag{12}$$

where $R_L(\omega_0)$ is the total load resistance connected to the output terminals of the transformer. When an extra resistance R_j is inserted in series with C_j, i.e., to the end of the cavity, provided that C_T is unaltered by this added resistance, $R_L(\omega_0)$ becomes

$$R_L(\omega_0) = R_c(\omega_0) + R_d \tag{13}$$

where

$$R_d = \frac{R_j}{\left(1+\frac{C_B}{C_j}\right)^2}. \tag{14}$$

Hence the normalized input impedance takes the form

$$\frac{Z_{\text{in}}(\omega_0)}{Z_o} = 1 + \frac{R_j}{R_c(\omega_0)\left(1+\frac{C_B}{C_j}\right)^2} = S \tag{15}$$

where S is the voltage standing-wave ratio. For different values of R_j, $Z_{\text{in}}(\omega_0)/Z_o$ lies on a straight line when plotted on the Smith chart. The plane PP cannot be found practically since $R_c=0$ condition is not possible. Instead, one can vary R_j by a known amount and calibrate Z_{in}/Z_o over a range which includes the value of the varactor loss resistance. From the measured values of a set of resistances, the value of R_c can also be determined. Since the diode resistance is of the order of R_c at UHF, the value of the standing-wave ratio will vary around 1 to 3, which is the most accurate region of the Smith chart. Fig. 4 shows Z_{in}/Z_o as plotted on the Smith chart.

A number of carbon resistors were made having almost the same dimensions as that of a pill-type varactor diode and their values were determined from dc to 2 GHz. In measuring these resistances no difficulties were encountered because no series capacitances are involved. The lossless capacitance was obtained by a variable gap at the end of the cavity.

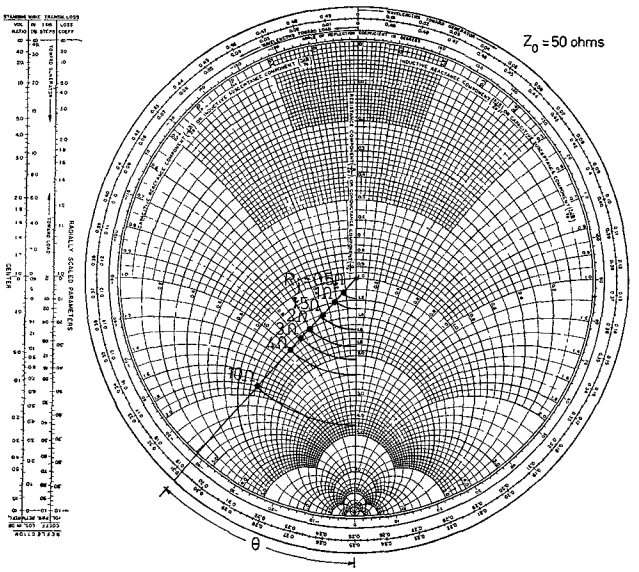

Fig. 4. Variation of Z_{in}/Z_o on the Smith chart for different values of R_j. θ is the angle between PP and the plane at which measurements are made.

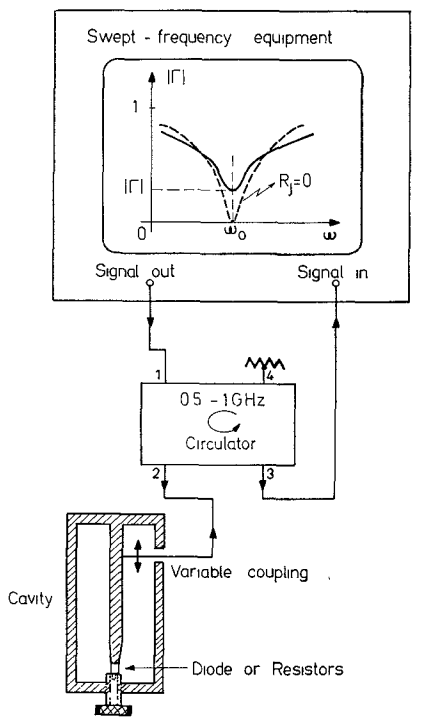

Fig. 5. Setup for measuring reflection coefficient by the swept-frequency technique.

Since the method requires exact substitution of C_j each time a new resistance or diode is inserted, the swept-frequency technique and the inclusion of a circulator into the measuring set will facilitate the measurements. Fig. 5 shows the measuring set for this purpose with which the reflection coefficient Γ is measured. Γ is given by

$$|\Gamma(\omega_0)| = \frac{S-1}{S+1} = \frac{1}{1+\frac{2R_c(\omega_0)}{R_j\left(1+\frac{C_B}{C_j}\right)^2}}. \tag{16}$$

TABLE I

MEASURED RESISTANCES OF VARIOUS VARACTOR DIODES AS A FUNCTION OF FREQUENCY

VARACTOR DIODE	FREQUENCY (MHz)					RESISTANCE (OHMS)
	300	500	700	900	1000	
Alpha Industries MO101CP C_j=0.67pf at OV	0.50	0.49	0.51	0.50	0.49	
Alpha Industries MO 303 AP C_j=2.5pf at OV	1.2	1.22	1.2	1.18	1.25	
Ferranti ZC20E C_j=11pf. at OV	2.1	1.9	2.0	2.05	1.95	
Ferranti ZC 29E C_j=0.85pf at OV	1.00	1.10	1.00	0.98	1.05	
Motorola (step recovery) MV1816B C_j=5pf at -10V	0.51	0.50	0.50	0.49	0.50	

The sequence of measurements is as follows.

1) Insert the diode into the cavity and adjust the cavity coupling until a near-match condition is obtained at a given ω_0.

2) Take the diode out and adjust the lossless capacitance at the end of the cavity until resonance occurs at the same frequency ω_0 as in 1) by watching on the scope of the swept-frequency equipment. Then fully match the cavity losses to Z_o at ω_0. The matched condition is obtained as the zero output from port 3 of the circulator of Fig. 5.

3) Insert known resistors and calibrate $|\Gamma|$ or S as measured in the input line at ω_0.

4) Insert the diode and read the corresponding $|\Gamma|$ or S. Since the diode and cavity stray elements and the cavity losses are not altered when the resistors are inserted, the values of the substituted resistors, as a consequence of (15) or (16), correspond to R_j directly.

Table I shows the measured series loss resistances of different varactor diodes using this method in the frequency region of 300–1000 MHz. No variation in the value of diode resistance with frequency could be observed.

IV. EFFECT OF VARACTOR CAPACITANCE ON NOISE TEMPERATURE OF PARAMETRIC AMPLIFIERS

It has been generally accepted that the static diode capacitance does not play a direct role on the noise performance of a parametric amplifier. In light of the results obtained in Section II, the circuit losses involved depend very much on the signal circuit tuning inductor required for resonance. Higher values of diode capacitance reduces the value of this inductor and hence the associated circuit losses. It is therefore expected that higher values of diode capacitance will result in lower noise temperatures. In Fig. 6 the signal-frequency equivalent circuit of a UHF circulator coupled negative-resistance parametric amplifier is shown. In this figure R_j and C_j are the loss resistance and the capacitance of the diode junction. C_B is the sum of the stray capacitances of the varactor diode, the capacitance due to the discontinuity of the inner conductor and the capacitance due to the idler choke. L_c and R_c are the inductance and the loss resistance of the signal cavity, and R_g is the source resistance transformed by the coupling of the cavity to the signal circuit. In the same figure the effect of C_B is taken into account in the series representation of the cavity across the diode junction. Since in the following noise analysis the diode junction is represented by a resistance in series with a capacitance [17], C_B results in the following impedance transformations:

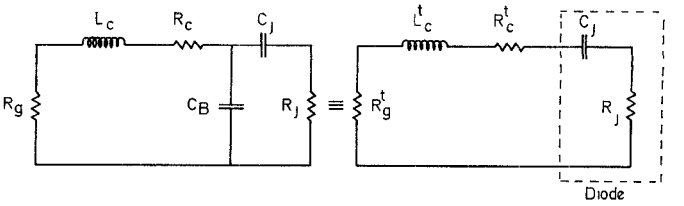

Fig. 6. Equivalent circuit of the signal side of a UHF parametric amplifier.

$$R_g^t(\omega) = R_g \frac{1}{(1 - \omega^2 C_B L_c)^2} \tag{17}$$

$$L_c^t(\omega) = L_c(\omega) \frac{1}{(1 - \omega^2 L_c C_B)} \tag{18}$$

$$R_c^t(\omega) = R_c(\omega) \frac{1}{(1 - \omega^2 L_c C_B)^2} \tag{19}$$

In the following calculation of the noise temperature of this amplifier as a function of frequency it is assumed that the gain is kept constant by varying the coupling to the signal cavity at each frequency.

The available resonant gain expression, in terms of the above parameters, becomes

$$G_a = \left[\frac{R_c^t + R_j - R_N - R_g^t}{R_c^t + R_j + R_g^t - R_N}\right]^2 \tag{20}$$

where R_N is the negative resistance which is given by [18]

$$-R_N = -\frac{\gamma^2}{\omega_0 \omega_2 C_j^2 R_{T2}} \tag{21}$$

where $\gamma = (C_1/C_j)$, C_1 being the first Fourier coefficient in the capacitance expansion and depends upon the pumping level and the type of the varactor diode. R_{T2} is the total idler loss resistance at the idler frequency ω_2. The necessity for constant gain results in a VSWR, $s(\omega_0)$ at the input terminals which will be obviously dependent on the resonant frequency. In the case of a parametric amplifier $s(\omega_0)$, which is defined as $s(\omega_0) > 1$, is given by

$$s(\omega_0) = \frac{R_g^t(\omega_0)}{R_c^t(\omega_0) + R_j}. \tag{22}$$

The effective noise temperature used in the calculations with the high gain approximation ($\geq$10 dB) is given by

$$T_{\text{eff}}(\omega_0) = \left[\frac{R_c^t(\omega_0) + R_j}{R_g^t(\omega_0)} + \frac{\omega_0}{\omega_2} \frac{R_g^t(\omega_0) + R_j + R_c^t(\omega_0)}{R_g^t(\omega_0)}\right] 290 \text{ K}. \tag{23}$$

In terms of the VSWR this expression reduces to

$$T_{\text{eff}}(\omega_0) = \left[s^{-1}(\omega_0) + \frac{\omega_0}{\omega_2}(s^{-1}(\omega_0) + 1)\right] 290 \text{ K}. \tag{24}$$

To obtain the variation of $T_{\text{eff}}(\omega_0)$ with ω_0 one has to know the values of γ and R_{T2}, which are difficult to determine. However, since the cavity losses are negligibly small after about 1 GHz, these coefficients can be obtained for a lossless signal cavity and for a given junction capacitance, and then used as constants for the analysis below 1 GHz.

$R_g{}^t(\omega_0)$ is obtained from (20) as

$$R_g{}^t(\omega_0) = [R_N(\omega_0) - R_c{}^t(\omega_0) - R_j]\left(\frac{G_a{}^{1/2} - 1}{G_a{}^{1/2} + 1}\right). \quad (25)$$

To obtain constant gain the necessity of changing $R_g{}^t$ when $R_c{}^t(\omega_0)$ is varying is evident from the above expression. This value of $R_g{}^t(\omega_0)$ is substituted in (22) to obtain

$$s^{-1}(\omega_0) = \left[\frac{R_c{}^t(\omega_0) + R_j}{R_N(\omega_0) - R_c{}^t(\omega_0) - R_j}\right]\left(\frac{G_a{}^{1/2} + 1}{G_a{}^{1/2} - 1}\right). \quad (26)$$

Substituting (26) into (24), T_{eff} is obtained as

$$T_{\text{eff}}(\omega_0) = \left\{\left(\frac{G_a{}^{1/2}+1}{G_a{}^{1/2}-1}\right) \Big/ \left[\left(\frac{R_N(\omega_0)}{R_c{}^t(\omega_0)+R_j} - 1\right)\right]\right.$$
$$\left. + \frac{\omega_0}{\omega_2}\left[\left(\frac{G_a{}^{1/2}+1}{G_a{}^{1/2}-1}\right) \Big/ \left(\frac{R_N(\omega_0)}{R_c{}^t(\omega_0)+R_j} - 1\right) + 1\right]\right\} 290 \text{ K}. \quad (27)$$

$R_c{}^t(\omega_0)$ is effected by the diode capacitances through (9) and (19) and decreases as both ω_0 and C_T increase.

Fig. 7 shows the computed values of $T_{\text{eff}}(\omega_0)$ from (27) as a function of ω_0 and as normalized to 1 GHz. The results are shown for different values of C_j. A change in C_j from 0.5 to 1 pF results in more than a three-fold improvement in the noise temperature in the lower end of UHF. In Fig. 8 the variation of $T_{\text{eff}}(\omega_0)$ is shown when the variable parameter is chosen to be the sum of the stray capacitances C_B. The improvement is more or less constant for the whole frequency region but not as much pronounced as in the case of increasing the value of C_j. In practice the addition of C_B is very undesirable since it degrades gain–bandwidth performance.

In an experimental parametric amplifier these results have been checked using varactor diodes having different junction capacitances. In Fig. 7 the expected noise temperature from the measured VSWR and related to the amplifier performance through (24), is also shown by broken lines.

V. Conclusions

The well-known frequency-dependent character of the varactor diode resistance is shown to be caused by the distributed circuit losses transformed across the diode. In a new measurement technique which is not effected by the circuit losses, the varactor diode resistance was shown to be frequency independent. In this measurement technique, although tedious to implement in practice, the use of a number of artifically made resistors is inevitable in order to attribute firm values to the diode resistance.

Since the general Weissfloch equivalent 2-port network includes both shunt and series loss resistances, representing all the losses in the 2-port cavity (Fig. 3) by a series resistance is an approximation and was inspired by the fact that externally added resistors do not perturb the resonant frequency of the cavity. The phenomenally constant resistance values of Table I may also be considered as a justification.

Towards the reduction of noise temperature of a parametric amplifier operated at UHF the selection of varactor diode capacitance is considered to be important. Higher values of junction capacitances reduces the length of the cavity and hence the involved losses. However, an unlimited increase in the diode capacitance would be unnecessary due to the fact that after a certain maximum value of varactor capacitance the circuit losses become negligible. Additional stray capacitance, on the other hand, in parallel with the varactor diode does not yield as much improvement in the noise temperature as in the case of increasing the junction capacitance. This is because while the cavity length decreases as strays increase, the losses and the source impedance are transformed to a higher level. The magnitude of the source resistance can be readjusted by the coupling to the cavity, but the transformed losses cannot be affected. This hence limits the available gain from the parametric amplifier, a result which causes poorer noise temperature as shown in the previous section.

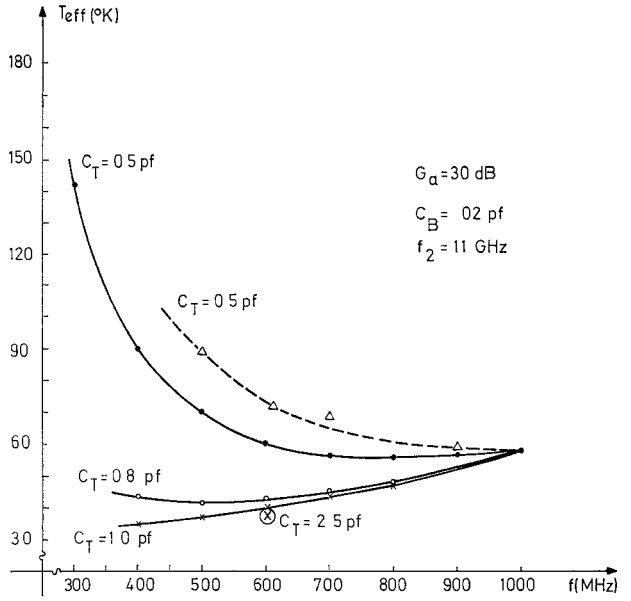

Fig. 7. Variation of T_{eff} with frequency for varactor diodes with different capacitances: ———— calculated, ---------- measured for ZC 20E, ⊗ measured for M0303AP.

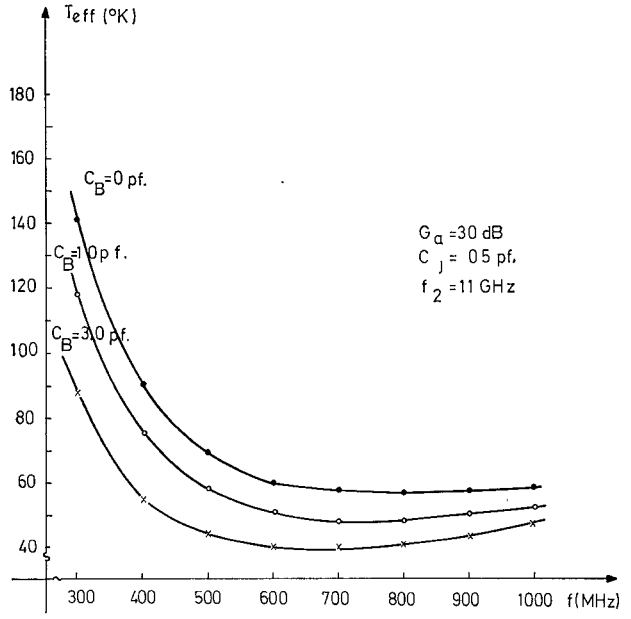

Fig. 8. Variation of T_{eff} with frequency for different values of the shunt stray capacitances.

References

[1] A. Uhlir, Jr., "Apparent frequency dependence of series resistance of varactor diodes," *Proc. IEEE* (Corresp.), vol. 51, pp. 1246–1247, Sept. 1963.

[2] L. D. Braun, "Frequency dependence of the equivalent series resistance of varactor diodes and its effect on parametric amplification,"

Proc. IRE (Corresp.), vol. 50, pp. 2523–2524, Dec. 1962.
[3] S. T. Eng and R. Solomon, "Frequency dependence of the equivalent series resistance for a germanium parametric amplifier diode," *Proc. IRE* (Corresp.), vol. 48, pp. 358–359, Mar. 1960.
[4] D. E. Sawyer, "Surface dependent losses in variable reactance diodes," *J. Appl. Phys.*, vol. 30, pp. 1689–1691, Nov. 1959.
[5] K. İnal and C. Toker, "Minimum noise figure of paramps with frequency dependent apparent R_s," *IEEE Trans. Microwave Theory Tech.* (Corresp.), vol. MTT-19, pp. 333–334, Mar. 1971.
[6] F. J. Hyde, S. Deval, and C. Toker, "Varactor diode measurements," *Radio Electron. Eng.*, vol. 31, pp. 67–75, Feb. 1966.
[7] R. I. Harrison, "Parametric diode Q measurements," *Microwave J.*, vol. 3, pp. 43–46, May 1960.
[8] R. Mavaddat, "Varactor diode Q-factor measurements," *J. Electron. Contr.*, vol. 15, pp. 51–54, July 1963.
[9] E. W. Sard, "A new procedure for calculating varactor Q from impedance versus bias measurements," *IEEE Trans. Microwave Theory Tech.*, vol. MTT-16, pp. 849–860, Oct. 1968.
[10] J. M. Roe, "Varactor Q measurement," *IEEE Trans. Microwave Theory Tech.* (Corresp.), vol. MTT-19, pp. 728–729, Aug. 1971.
[11] B. C. DeLoach, "A new microwave measurement technique to characterize diodes and an 800-Gc cutoff frequency varactor at zero volts bias," *IEEE Trans. Microwave Theory Tech.*, vol. MTT-12, pp. 15–20, Jan. 1964.
[12] C. Toker and F. J. Hyde, "The series resistance of varactor diodes," *Radio Electron. Engr.*, vol. 32, pp. 165–168, Sept. 1966.
[13] W. J. Getsinger, "The packaged and mounted diode as a microwave circuit," *IEEE Trans. Microwave Theory Tech.*, vol. MTT-14, pp. 58–69, Feb. 1966.
[14] H. N. Dawirs, "Equivalent circuit of a series gap in the center conductor of a coaxial transmission line," *IEEE Trans. Microwave Theory Tech.* (Corresp.), vol. MTT-17, pp. 127–129, Feb. 1969.
[15] T. Morena, *Microwave Transmission Design Data.* New York: Dover, 1958.
[16] E. L. Ginzton, *Microwave Measurements.* New York: McGraw-Hill, 1957, p. 279.
[17] D. G. Vice, "Parametric amplifier noise analysis," *IEEE Trans. Microwave Theory Tech.*, vol. MTT-13, pp. 162–167, Mar. 1965.
[18] L. H. Blackwell and K. L. Kotzebue, *Semiconductor Diode Parametric Amplifiers.* Englewood Cliffs, N. J.: Prentice-Hall, 1961.

A Moment Method with Mixed Basis Functions for Scatterings by Waveguide Junctions

Y. LEONARD CHOW AND SIEN-CHONG WU

***Abstract*—A moment method with mixed basis functions is introduced. In this formulation, modal basis functions are used for the expansion of the currents corresponding to the scattered propagating modes, while pulse basis functions are used for the expnsion of the current corresponding to the scattered envancescent waves. This, together with the Dirac δ weighting functions, reduces the number of total basis functions needed while retaining the simplicity and versatility of the method to cover junctions of an arbitrary shape. This method is applied to study examples of homogeneous and inhomogeneous waveguide junctions of parallel-plate waveguide propagating TE waves. It is found that for junctions that are not electrically large the convergence of the solutions is good.**

An appendix is included to transform and quicken the numerical integration of the modal basis functions.

I. Introduction

MOMENT METHODS have been used to study scattering problems for different types of scattering boundaries with accurate results. However, the basis functions used in each method have been limited to a single type. For instance, the unit-pulse basis functions have been used in the scattering by cylindrical obstacles in open space [1], [2]; the modal basis functions have been used in the scattering by two-dimensional (i.e., parallel-plate) waveguide diaphragms [3]–[5]. The former basis functions had to be used due to the "not-so-regular" shape of the cylindrical obstacle; the latter had to be used due to the infinite waveguide walls. From the above examples, it becomes evident that a mixed type of basis functions, consisting of both the unit pulses and the modes, would well be used for a cylindrical obstacle (along the third dimension) in a parallel-plate waveguide.

A first attempt in this direction for a single propagating TE_{10} mode was carried out by Wu and Chow [6]. In the present paper, the purpose is to extend and formulate TE modes of the parallel-plate waveguide in general, using the mixed basis functions, and along the same line as the standard formulation given by Harrington [1]. After the terms in the waveguide integral equation are identified with the basis functions, the scattering by a cylindrical obstacle (in waveguides, regular sized and oversized, with several propagating modes) is studied. The method is then applied to the scattering by a inhomogeneous waveguide junction with two different dielectrics. For convenience in both studies, the point-matched weighting functions are used.

Only a *small* number of basis functions are needed for the moment method using the mixed basis functions. The reason is the following. One type of the basis functions is used to represent the propagating modes along the infinite waveguide walls; there are only a few of these propagating modes. The other type (say, the narrow unit-pulse functions) is used to represent the evanescent waves; the evanescent waves are highly localized at the obstacle.

The numerical integration of the basis functions of the propagating mode is simplified and quickened by a field transformation. The derivation of the transformation is presented in the Appendix.

Manuscript received August 7, 1972; revised January 8, 1973. This work was supported by the National Research Council of Canada under Operating Grant A3804.

The authors are with the Department of Electrical Engineering, University of Waterloo, Waterloo, Ont., Canada.